Chalcogenide Fullerenes

DOI: 10.1002/anie.200902481

Snapshots of the Formation of Inorganic MoS_2 Onion-Type Fullerenes: A "Shrinking Giant Bubble" Pathway**

*Aswani Yella, Martin Panthöfer, Michael Kappl, and Wolfgang Tremel**

Dedicated to Professor Martin Jansen on the occasion of his 65th birthday

Fullerenes and nanotubes (NTs) have been increasingly investigated in the past decade and become symbols of the new and fast developing area of nanotechnology.[1] It is therefore surprising that we know very little today about the atomic-level formation mechanisms of these self-assembled hollow carbon nanostructures. Numerous efforts have been made in this respect during the past two decades.[1,2] One of the current models is the "shrinking hot giant" road of fullerene formation, which consists of two parts: a "size-up" part, in which giant fullerenes self-assemble by an interplay of dynamics and chemistry of hot polyyne chains in carbon vapor leading to formation of more or less curved sp^2 networks, and a "size-down" part, in which these giant, vibrationally excited cages shrink to the size of conventional fullerenes such as C_{60}.[3] Direct evidence for shrinkage of hot giant fullerenes was obtained by in situ high-resolution transmission electron microscopy (HRTEM).[4] The formation mechanism of carbon onions consisting of multishell concentric giant fullerenes has remained even more enigmatic since their discovery by Iijima[5] in 1980. These onion structures are formed typically under harsh conditions such as high-energy electron irradiation of a carbon precursor[6] on a carbon target in water.[7] A few conceptual growth models have been proposed for the nucleation and growth of carbon onions. Iijima and Ugarte proposed a sequential growth model in which a single closed fullerene emerged in a first step, and concentric shells successively formed around this seed fullerene subsequently.[5,6] An alternative spiral-like growth mechanism was suggested by Kroto and co-workers,[8] but even within each of these growth models, different pathways were proposed.[9]

In analogy to the nested carbon fullerenes and nanotubes, Tenne and co-workers[10,11] discovered related MQ_2-based (M = early transition metal; Q = S, Se) concentric closed-shell materials which laid the foundation for the entire field of nanostructures based on inorganic materials.[12] Meanwhile, chalcogenide nanoparticles have found application as solid lubricants,[13] heterogeneous catalysts,[14] super shock absorbers,[15] and battery materials.[16]

The analogy to the carbon fullerene family, however, falls short because no small preferred structure akin to C_{60} has been found. About ten years ago Parilla et al.[17] discovered nano-octahedra of MoS_2 of discrete sizes in soots that were prepared by laser ablation of pressed MoS_2 targets. Although these nano-octahedra are much larger than the prototypic C_{60} structure, that is, 1 nm for C_{60} and 4–5 nm for the nano-octahedra, they may represent the "true inorganic fullerenes". More recently, a experimental/theoretical analysis of the MoS_2 nano-octahedra[18] gave additional support for this hypothesis. Nano-octahedra consisting of 3–5 layers of MoS_2 with an atom count between about 10^3 and up to 8×10^4 proved be stable structures. Beyond 10^5 atoms, MoS_2 nanotubes and quasispherical nanoparticles are predicted to be stable forms of MoS_2 nanoparticles.[18]

Similar to their carbon congeners the chalcogenide onion-type nested fullerenes and nanotubes are not equilibrium but high-temperature and low-pressure phases in the W–S phase diagram that are obtained by quenching "hot" gas-phase species. Various synthetic approaches to so-called inorganic fullerenes (IFs) have been established so far, such as oxide-to-sulfide conversion,[19] decomposition of suitable precursors,[20] transport reactions,[21] laser or solar ablation,[22] and chemical vapor deposition (CVD).[23] Except for oxide-to-sulfide conversion, which has been scrutinized,[24] the growth mechanism of such nanostructures is still subject to discussion.

The formation mechanism of nested chalcogenide onions is still very poorly understood. Recently, we reported an in situ heating TEM study on the formation of IF-WS_2 and IF-MoS_2 from amorphous MoS_2 and WS_2 precursor nanoparticles obtained by metal–organic CVD (MOCVD).[25] In the growth of these onionlike particles defect annealing processes play a prominent role. In contrast, particles annealed ex situ showed more facile particle growth and higher crystallinity due to enhanced surface diffusion in the surrounding Ar gas atmosphere.

In order to trap reaction intermediates of nested fullerene formation, the reaction must be kinetically controlled, that is,

[*] A. Yella, Dr. M. Panthöfer, Prof. Dr. W. Tremel
Institut für Anorganische Chemie und Analytische Chemie
Johannes Gutenberg-Universität
Duesbergweg 10–14, 55099 Mainz (Germany)
Fax: (+49) 6131-39-25605
E-mail: tremel@uni-mainz.de
Dr. M. Kappl
Max Planck-Institut für Polymerforschung
Ackermannweg 10, 55128 Mainz (Germany)

[**] This work was supported by the Deutsche Forschungsgemeinschaft (DFG) within the priority program 1165 "Nanotubes and Nanowires: From Controlled Synthesis to Function". A.Y. is a recipient of a fellowship from POLYMAT, the Graduate School of Excellence of the State of Rhineland-Palatinate. We acknowledge the help of Dr. Enrico Mugnaioli with the EDX analysis and G. Glaßer with the SEM as well as support from the Materials Science Center (MWFZ) in Mainz.

Supporting information for this article is available on the WWW under http://dx.doi.org/10.1002/anie.200902481.

solid-state diffusion must be excluded as the rate-determining step. This can be achieved either by shortening the diffusion pathway, that is, making the particles small, or by enhancing atom mobility by adding a suitable mineralizing agent. Herein we describe the formation of giant MoS_2 "bubbles" with a controlled shell thickness of about 5 nm and void sizes around 120 nm through enhancement of surface diffusion with iodine. These giant IF-type structures are reaction intermediates obtained by quenching of the reaction through a large temperature gradient. These giant IF particles transform into "conventional" nested fullerenes and tubelike structures containing embedded IF particles upon subsequent annealing. Our results suggest giant IF particles not only to be intermediates of a "size-up" step on a "shrinking hot giant" road to nested chalcogenide fullerenes, but also intermediates in chemical transport reactions of layered chalcogenides.

Giant IF-MoS_2 particles were synthesized by using a setup described for the synthesis of IF-MoS_2.[23a] The $Mo(CO)_6$ precursor was replaced by a mixture of $Mo(CO)_6$ and I_2. While the molecular precursors $Mo(CO)_6$ and I_2 were heated to 150 °C in all experiments, the temperature of the hot reactor zone was varied from 450 to 650 °C in steps of 100 °C for different sets of experiments. A constant reaction time of 1 h was used for the MOCVD step in all experiments. After purging the reactor with argon, the graphite receptor was heated inductively to the respective reaction temperature (temperature at the graphite receptor $250 < T_{ind} < 650$ °C). Once the appropriate reaction temperature was reached, the precursors were heated with heating rates chosen such as to assure a homogeneous reaction mixture for the duration of the experiment. The possibility of fast heating/cooling of the reaction zone makes this induction-heated setup advantageous as compared to the slow temperate ramps achievable with tube furnaces, because "quenching" of the reaction is possible at any time. This allowed the structure of the reaction products to be monitored as a function of the reaction time by taking samples after given time intervals. The samples obtained from the MOCVD setup were annealed in a horizontal tube furnace at the 850 °C (heating rate 5 °C min^{-1} under constant argon gas flow of 100 cm^3-(STP) min^{-1} for 1 h).

Annealing of the products obtained at different temperatures resulted in the formation of different IF nanostructures. The precursor products obtained from the reaction of $Mo(CO)_6$, I_2, and H_2S gas at T_{ind} values of 350 and 450 °C were amorphous. The TEM images of these precursor particles obtained at 350, 450, and 550 °C are presented in Figure 1. The product mainly consists of spherical MoS_2 particles with diameters of 15–20 nm. The precursor particles look similar to those obtained without using iodine. X-ray powder diffraction and HRTEM analysis on the precursor particles reveal the product to be almost amorphous for samples prepared at 350 and 450 °C. An energy-dispersive X-ray analysis indicated the presence of iodine, which, however, proved difficult to quantify because of its volatility.

Differential scanning calorimetry/thermogravimetric (DSC/TG) measurements were performed under argon at a heating rate of 20 °C min^{-1}. The sample displayed a small endothermic effect in the DSC trace. The TG data revealed a continuous weight loss (total of 57 %) with two discernable steps at 285 and 445 °C corresponding to weight losses of 18 and 57 %, respectively. This corresponds to thermal decomposition with loss of iodine. The formation of a "solid solution" is indicated by the gradual weight loss, whereas formation of a single phase would be indicated by a stepped TG trace. HRTEM analysis on the precursor particles obtained at 550 °C revealed very few layers of MoS_2 which are not arranged in an ordered fashion (Figure 1 d).

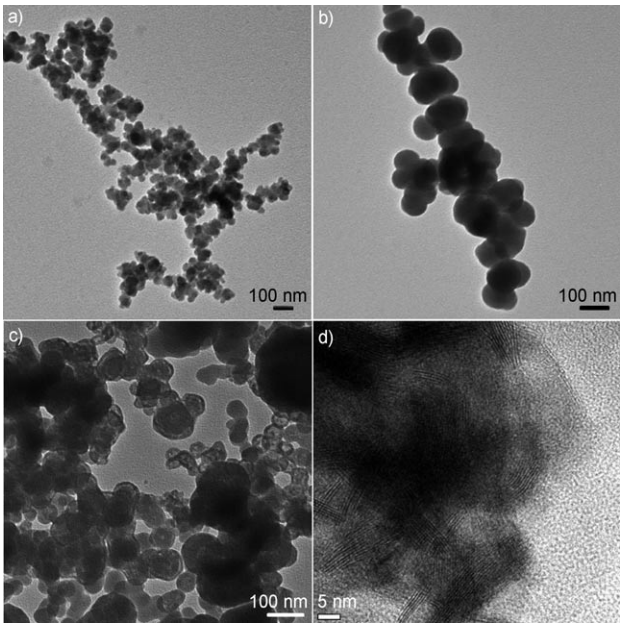

Figure 1. TEM images of the precursor particles obtained from the MOCVD setup at reaction temperatures of a) 350, b) 450, and c) 550 °C. d) HRTEM image of a precursor particle obtained at 550 °C.

Subsequently, the precursor particles obtained at different reaction temperatures were annealed at 850 °C under argon flow for 30 min. After this annealing step the crystallinity of the product had improved, and its composition was determined by X-ray powder diffraction (see Figure 2). All reflections could be attributed to 2H-MoS_2 and a minor amount of an $Mo_2S_5I_3$ impurity.[26]

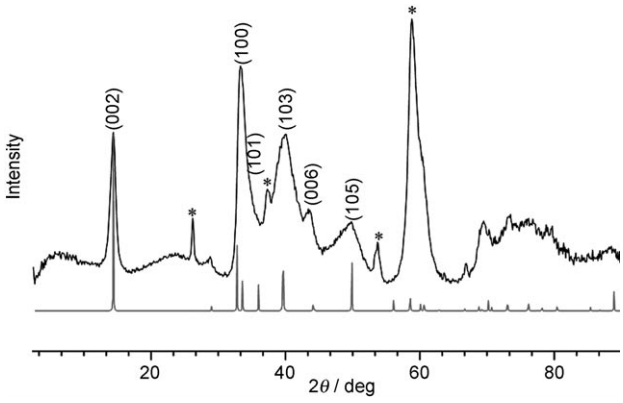

Figure 2. X-ray powder diffractogram of the product obtained after annealing at 850 °C. (line pattern: 2H-MoS_2). Reflections marked by * correspond to $Mo_2S_5I_3$ impurities.[26]

The TEM images of the product obtained after annealing showed fullerene-like particles which are very different from those that were obtained in the absence of iodine (Figure 3).

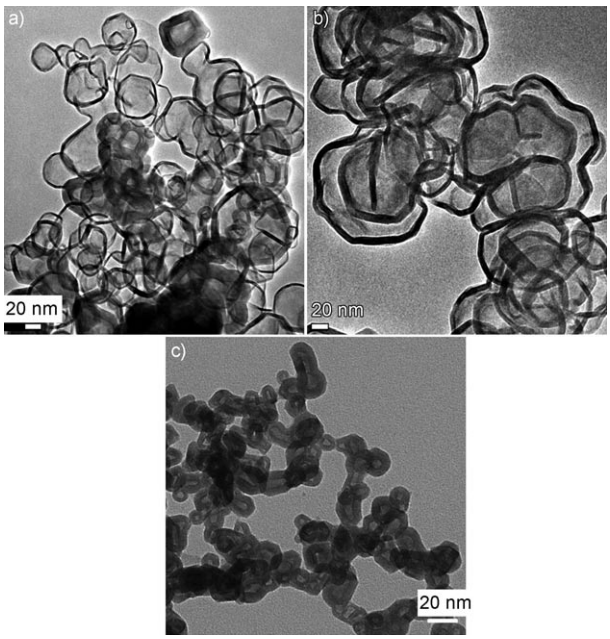

Figure 3. Overview TEM images of the product obtained after annealing the precursor particles obtained at a) 350, b) 450, and c) 550 °C for 30 min at 850 °C under argon flow.

In general, these hollow IF fullerenes have thin walls (about 5–6 layers) of MoS_2 with a large empty interior space, resembling a soccer ball. During the annealing process the diameter of the precursor particles had increased substantially, and the diameter was dependent on the reaction temperature, that is, on the iodine content of the precursor particles. The product obtained from the precursor particles prepared at 350 °C resembled giant IF nanostructures with particle diameters on the order of 120 nm. The product obtained by annealing precursor particles prepared at 450 °C consisted of large IF fullerene particles containing considerably smaller IF fullerenes inside, while that obtained by annealing precursor particles prepared at 550 °C consisted of IF fullerene-type particles which are strongly interconnected in a chain-type fashion.

The HRTEM images of the products obtained after annealing of the precursor particles synthesized at 350, 450, and 550 °C are presented in Figure 4. The interlayer spacing in all giant IF-nanoparticles was 0.61 nm, which matches well with the interlayer distance of MoS_2. An EDX analysis showed no evidence for the presence of iodine. Thus, the iodine contained in the intermediate products had sublimed completely, reminiscent of calcination reactions in sol–gel syntheses. Fullerenes prepared from precursors synthesized at 350 and 450 °C displayed very thin walls with only few, but highly crystalline, layers of MoS_2 (see Figure 4). Annealing of the precursor obtained at 550 °C led to tubelike structures containing embedded nested fullerene-type particles reminiscent of nanopods (Figure 4c and d), which bear some

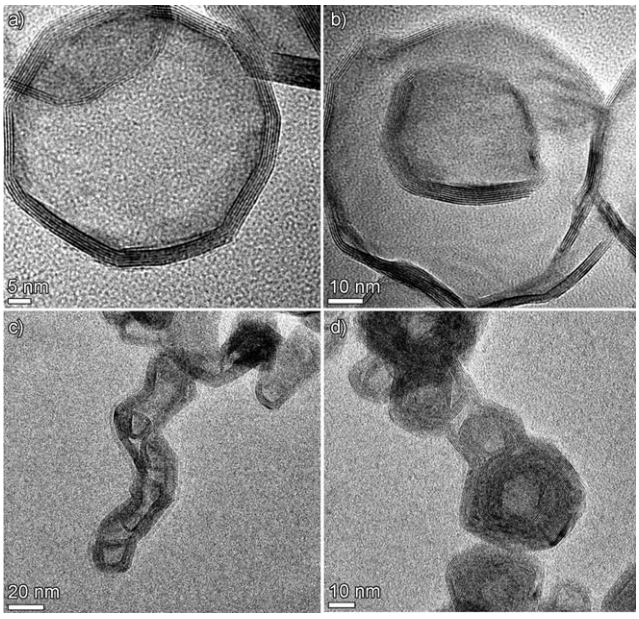

Figure 4. HRTEM images of the product obtained after annealing the precursor particles at a) 350, b) 450, c) 550 °C, and d) 650 °C for 30 min at 850 °C under argon flow.

resemblance to nanostructures obtained by treating $Mo_6S_2I_8$[27] with $H_2S/H_2/Ar$ at 1100 K.[28] These nanopodlike structures appear to be a result of annealing the chain-type precursor particles. The iodine content of the precursor particles decreases with increasing reaction temperature. The product obtained at 550 °C bears some resemblance to the product obtained at 450 °C when the reaction is performed without iodine.

Upon annealing, the amorphous precursor particles transformed into large hollow particles with giant IF-fullerene-type architecture. The formation of the large interior voids may be traced back to formation of gas-phase species through thermal decomposition of the amorphous ternary Mo–S–I precursor phase. Part of the vapor phase (iodine) is trapped within the newly forming IF-fullerene-like structure. Upon annealing, thermal decomposition of the precursor particles proceeds while, at the same time, the vapor pressure within the fullerene increases. This leads to a "size-up" effect through thermal expansion of the encapsulated gas phase, whereby the forming fullerene particle is stable as long as the pressure inside the fullerene remains below a threshold "burst" value. At the same time the iodine vapor within the fullerene leads to the formation of a surface film that makes the molybdenum and sulfur atoms mobile by isothermal chemical-transport reaction of the halogen in the surface film. Steady loss of iodine to the gas phase promotes formation of nuclei on the surface and thus leads to enhanced and accelerated rebuilding of the IF-MoS_2 fullerene shell. Surface diffusion requires considerably lower activation energy than solid diffusion, and consequently it is operative at lower temperatures. The diffusion constants for surface diffusion correspond in magnitude to those in solutions and in melts. The intermediate stages observed are shown in Figure S1 of the Supporting Information.

This reaction mechanism cannot work under vacuum, because the necessary surface film cannot be formed. In this case thermal decomposition can only proceed smoothly when solid diffusion is rapid enough, that is, at elevated temperatures ($T \approx 900\,^{\circ}C$). In accordance with this interpretation, it is found from X-ray powder diffraction and electron microscopy that IF-MoS_2 obtained from the Mo-S-I precursor phase is well crystallized and well ordered to 2H-MoS_2, while that obtained under the conditions of in situ heating TEM under high vacuum[25] display a significantly higher defect density. In agreement with this, it is also found that only intermediate temperatures ($350 < T < 550\,^{\circ}C$) are required for the formation of the giant fullerene structures, whereas temperatures above 850 °C are needed for in situ heating TEM under high vacuum.

Thermal decomposition of the amorphous precursor and the concomitant loss of iodine to the gas phase must be accompanied by the buildup of a gas pressure inside the giant fullerenes. When the vapor pressure inside the fullerene shells increases above a "burst-threshold" value, the shell starts collapsing and the gas contained in the "bubble" IF-fullerene is released. The burst-threshold value will depend not only on the internal gas pressure, but also on the surface tension and the elastic properties of the chalcogenide shell. The first "size-down" step leads to formation of smaller IF fullerenes encapsulated in giant IF-fullerene cages (Figure 4b). In the next step the giant IF-fullerenes disintegrate into several giant IF-fullerenes particles, and the smaller particles are now contained in tubular structures (Figure 4c). This image indicates that tubelike structures containing embedded nested fullerenes are reaction intermediates in the formation of nanotubes on a "shrinking hot giant" pathway. Further increase of the temperature leads to the formation of twinned IF-fullerene structures which, in the final step, transform into the well-known onion-type fullerenes. The individual steps are illustrated and summarized in Scheme 1. Figure 5 shows an overview SEM image of the sample obtained at 350 °C after annealing.

Assuming the first reaction step takes place without any loss of iodine and leads to an homogeneous distribution of iodine within the MoS_2 hollow spheres, approximately 3.22×10^{-15} mmol of iodine is contained inside a MoS_2 sphere with an inner diameter of 50 nm, an outer diameter of 55 nm, and a corresponding volume of 6.5×10^{-17} mL. In the range from 400 to 800 °C the vapor from a mixture of MoS_2 and I_2 was reported to consist exclusively of I_2.[29] Neither molybdenum iodide nor atomic iodine is present. Based on this scenario, the pressure at 400 °C inside a MoS_2 sphere is as high as 1.1 kbar. This unexpectedly high pressure inside the MoS_2 hollow spheres strongly supports the proposed scenario of pressure-driven expansion and final explosion of the MoS_2 hollow spheres.

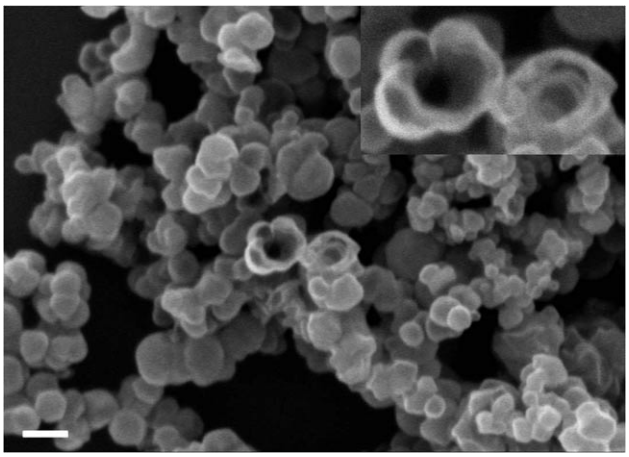

Figure 5. Overview SEM image of the sample obtained after annealing at 900 °C. The inset clearly shows a burst particle which could not close because the burst pressure was too high or the volume to be repaired was too large.

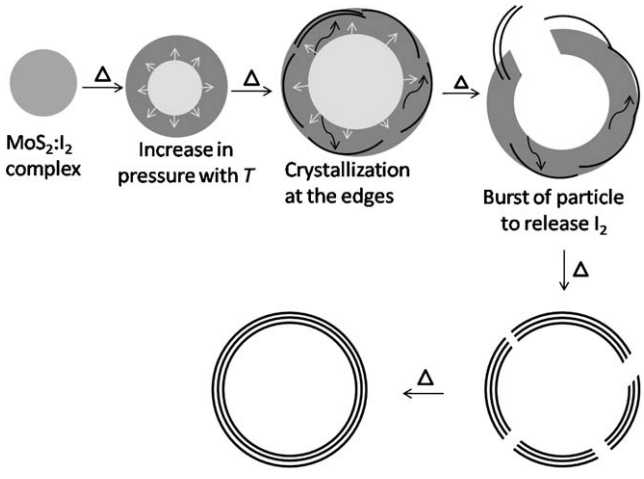

Scheme 1. Growth mechanism of a giant IF-MoS_2 fullerene.

Raman spectra were recorded at ambient temperature with 532.21 nm laser excitation line, and the spectra (Figure S2, Supporting Information) were compared to the reported data for IF-MoS_2[30] and NT-MoS_2.[31] The spectra exhibit similar peak positions as observed for NT-MoS_2. Raman spectra of IF-MoS_2[30] show additional bands compared to the spectra of bulk MoS_2, which are believed to originate from disorder effects. The absence of these vibration bands in our samples indicates a low defect density and a high degree of order within the layers, which can be explained by the high mobility of the constituents during nanoparticle formation.[32]

The strength of the shells was estimated by atomic force microscopy (AFM).[33] Tapping-mode imaging was used to locate the spheres on the substrate and to position the AFM tip on top of the center of the sphere. Deflection versus piezo extension curves were recorded on top of the spheres. Reference curves were recorded on the hard substrate next to the spheres in order to obtain the conversion factor to convert the observed detector deflection signal in volts to cantilever deflection in nanometers by fitting the linear contact part of the force curve. This conversion factor, together with the spring constant of the cantilevers, was used to determine the force versus indentation relation for the MoS_2 spheres, assuming that the deformation of the hard substrate is negligible. An example of such force versus

distance curve is shown in Figure S2 (Supporting Information). At large distances, no force acts between tip and sphere. At close approach, tip and sphere jump into contact as the gradient of the attractive forces overcomes the spring constant of the AFM cantilever. Further approach leads to deformation of the sphere by the AFM tip. For small applied loads of 5–10 nN, a linear relation between load and deformation was observed, in agreement with the thin-shell model (Figure S3, Supporting Information). For higher applied loads, the indentation curve becomes nonlinear (Figure S4, Supporting Information) and at even higher loads a buckling of the spheres occurs (Figure S5, Supporting Information). Buckling does not lead to destruction of the spheres, because curves as in Figure S5 of the Supporting Information can be recorded repeatedly without any significant change. From the AFM measurements an average stiffness value (F/d) of $1.3 \pm 0.7\ \mathrm{nN\,nm^{-1}}$ was extracted. With a sphere diameter of 80 nm and a shell thickness of 4 nm and a Poisson ratio of 0.3, this corresponds to a Young's modulus of $E = 1.33 \pm 0.7$ GPa which describes the elastic behavior of the giant IF-MoS_2 nanoparticles. This compares with Young's moduli of 230 ($\parallel c$) and 52 GPa ($\perp c$) for bulk MoS_2,[34] and of about 170 and 150 GPa for WS_2 nanotubes,[35] obtained from buckling tests under both atomic force and scanning electron microscopes. The data show that the elastic modulus changes dramatically in the narrow diameter range (20–80 nm). An even more drastic diameter dependence, with a difference of about two orders of magnitude in the 10–20 nm diameter range, has been reported for multiple-wall carbon nanotubes (MWCNTs, thinner MWCNTs have higher elastic modulus).[36] Whereas the burst pressure of the giant IF particles reported in this work is about 1.1 kbar = 0.11 GPa, IF-MoS_2 particles with diameters of 20–30 nm were reported to withstand a shock pressure of about 25 GP.[37] Together with the diameter dependence of the Young's modulus this is further support for the proposed scenario of pressure-driven expansion and final explosion of the MoS_2 hollow spheres.

In conclusion, we have demonstrated a novel approach to unraveling the formation mechanism of nested MoS_2 fullerenes by taking TEM snapshots of reaction intermediates that were obtained by annealing amorphous Mo–S–I nanoparticle precursors captured from an MOCVD reaction. The MOCVD approach allows not only trapping of reaction intermediates by thermal quenching, but also facile control of the reaction process and monitoring of particle growth by the choice of the experimental conditions (precursor etc.). Our strategy herein was to use amorphous Mo–S–I precursor nanoparticles to exclude solid-state diffusion as a rate-determining step in the formation of nested fullerenes. Thermal decomposition of the precursors at 350 °C led in the first step to the formation of giant fullerenes with diameters greater than 150 nm bounded by 5–6 chalcogenide layers, whereby the "size-up" step may be caused by a "bubble effect" from the gas phase participating in the reactions. On increasing the temperature to 450 °C and higher, smaller fullerene particles segregate within these giant fullerenes, and a "shrink-down" process leads to the formation of tubular MoS_2 structures containing embedded nested fullerene particles. In the final steps, twinned IF fullerenes and nested fullerene particles are formed. Our results bear resemblance to the "shrinking hot giant" model of carbon fullerene formation.[3] The above results also suggest that nanopod structures may be considered as possible reaction intermediates for the formation of multiple-wall nanotubes.[38] In addition, trapping of giant fullerenes from the Mo–S reaction system under conditions of isothermal chemical transport with iodine indicates the possibility that these (or similar nanostructures) are present as polynuclear intermediates or gas-phase complexes[32,39] in corresponding transport reactions.

Received: May 10, 2009
Revised: August 14, 2009
Published online: March 4, 2010

Keywords: chalcogens · fullerene-like materials · molybdenum · nanoparticles · nanotubes

[1] M. S. Dresselhaus, G. Dresselhaus, P. C. Eklund, *Science of Fullerenes and Carbon Nanotubes*, Academic Press, San Diego, **1996**.
[2] R. E. Smalley, *Acc. Chem. Res.* **1992**, *25*, 98–105.
[3] S. Irle, G. S. Zheng, Z. Wang, K. Morokuma, *J. Phys. Chem. B* **2006**, *110*, 14531–15545.
[4] J. Y. Huang, F. Ding, K. Jiao, B. I. Yakobson, *Phys. Rev. Lett.* **2007**, *99*, 175503.
[5] S. Iijima, *J. Cryst. Growth* **1980**, *50*, 675–683.
[6] D. Ugarte, *Nature* **1992**, *359*, 707–709.
[7] N. Sano, H. Wang, I. Alexandrou, M. Chhowalla, K. B. K. Teo, G. A. J. Amaratunga, *J. Appl. Phys.* **2002**, *92*, 2783–2788.
[8] H. W. Kroto, K. McKay, *Nature* **1988**, *331*, 328–331.
[9] a) D. Ugarte, *Carbon* **1995**, *33*, 989–993; b) D. W. M. Lau, D. G. McCulloch, N. A. Marks, N. R. Madsen, A. V. Rode, *Phys. Rev. B* **2007**, *75*, 233408.
[10] a) R. Tenne, L. Margulis, M. Genut, G. Hodes, *Nature* **1992**, *360*, 444–446; b) L. Margulis, G. Salitra, R. Tenne, M. Talianker, *Nature* **1993**, *365*, 113–115.
[11] Y. Feldman, E. Wasserman, D. J. Srolovitz, R. Tenne, *Science* **1995**, *267*, 222–225.
[12] R. Tenne, G. Seifert, *Annu. Rev. Mater. Res.* **2009**, *39*, 1–27.
[13] a) L. Rapoport, Yu. Bilik, Y. Feldman, M. Homyonfer, S. R. Cohen, R. Tenne, *Nature* **1997**, *387*, 791; b) M. Chhowalla, G. A. J. Amaratunga, *Nature* **2000**, *407*, 164–165.
[14] a) P. Afanasiev, L. Rawas, M. Vrinat, *Mater. Chem. Phys.* **2002**, *73*, 295–300; b) J. V. Lauritsen, J. Kibsgaard, S. Helveg, H. Topsøe, B. S. Clausen, E. Lægsgaard, F. Besenbacher, *Nat. Nanotechnol.* **2007**, *2*, 53–58.
[15] Y. Q. Zhu, T. Sekine, Y. H. Li, M. W. Fay, Y. M. Zhao, C. H. P. Poa, W. X. Wang, M. J. Roe, P. D. Brown, N. Fleischer, R. Tenne, *J. Am. Chem. Soc.* **2005**, *127*, 16263–16272.
[16] A. Zak, Y. Feldman, V. Lyakhovitskaya, G. Leitus, R. Popovitz-Biro, E. Wachtel, H. Cohen, S. Reich, R. Tenne, *J. Am. Chem. Soc.* **2002**, *124*, 4747–4758.
[17] P. A. Parilla, A. C. Dillon, K. M. Jones, G. Riker, D. L. Schulz, D. S. Ginley, M. J. Heben, *Nature* **1999**, *397*, 114.
[18] A. N. Enyashin, S. Gemming, M. Bar-Sadan, R. Popovitz-Biro, S. Y. Hong, Y. Prior, R. Tenne, G. Seifert, *Angew. Chem.* **2007**, *119*, 631–635; *Angew. Chem. Int. Ed.* **2007**, *46*, 623–627.
[19] a) A. Rothschild, R. Tenne, J. Sloan, A. P. E. York, M. L. H. Green, J. L. Hutchison, *Chem. Commun.* **1999**, 363–364; b) W. K. Hsu, Y. Q. Zhu, N. Yao, S. Firth, R. J. H. Clark, H. W. Kroto, D. R. M. Walton, *Adv. Funct. Mater.* **2001**, *11*, 69–74; c) X. L. Li, Y. D. Li, *Chem. Eur. J.* **2003**, *9*, 2726–2731; d) H. A.

Therese, J. X. Li, U. Kolb, W. Tremel, *Solid State Sci.* **2005**, *7*, 67 – 72; e) H. A. Therese, N. Zink, U. Kolb, W. Tremel, *Solid State Sci.* **2006**, *8*, 1133 – 1137; f) M. Remskar, M. Virsek, A. Jesih, *Nano Lett.* **2008**, *8*, 76 – 80.

[20] a) C. M. Zelenski, P. K. Dorhout, *J. Am. Chem. Soc.* **1998**, *120*, 734 – 742; b) M. Nath, A. Govindaraj, C. N. R. Rao, *Adv. Mater.* **2001**, *13*, 283 – 287; c) Y. Q. Zhu, W. K. Hsu, H. Terrones, N. Grobert, B. H. Chang, M. Terrones, B. Q. Wei, H. W. Kroto, D. R. M. Walton, C. B. Boothroyd, I. Kinloch, G. Z. Chen, A. H. Windle, D. J. Fray, *J. Mater. Chem.* **2000**, *10*, 2570 – 2577.

[21] a) M. Remskar, A. Mrzel, Z. Skraba, A. Jesih, J. Demsar, P. Stadelman, F. Levy, D. Mihailovic, *Science* **2001**, *292*, 479 – 481; b) M. Remskar, A. Mrzel, R. Sanjines, H. Cohen, F. Levy, *Adv. Mater.* **2003**, *15*, 237 – 240.

[22] a) M. Nath, C. N. R. Rao, R. Popovitz-Biro, A. Albu-Yaron, R. Tenne, *Chem. Mater.* **2004**, *16*, 2238 – 2240; b) J. M. Gordon, E. A. Katz, D. Feuermann, A. Albu-Yaron, M. Levy, R. Tenne, *J. Mater. Chem.* **2008**, *18*, 458 – 462.

[23] a) J. Etzkorn, H. A. Therese, F. Rocker, N. Zink, U. Kolb, W. Tremel, *Adv. Mater.* **2005**, *17*, 2372; b) N. Zink, J. Pansiot, J. Kieffer, H. A. Therese, M. Panthöfer, F. Rocker, U. Kolb, W. Tremel, *Chem. Mater.* **2007**, *19*, 6391 – 6400; c) A. Yella, H. A. Therese, M. Panthöfer, W. Tremel, *Chem. Mater.* **2008**, *20*, 3587 – 3593.

[24] a) R. Tenne, M. Homyonfer, Y. Feldman, *Chem. Mater.* **1998**, *10*, 3225 – 3238; b) R. Tenne, *Chem. Eur. J.* **2002**, *8*, 5297 – 5305.

[25] N. Zink, H. A. Therese, J. Pansiot, A. Yella, F. Banhart, W. Tremel, *Chem. Mater.* **2008**, *20*, 65 – 71.

[26] C. Perrin, A. Perrin, J. Prigent, *Bull. Soc. Chim. Fr.* **1972**, *8*, 3086 – 3091. Attempts to produce pure $Mo_2S_5I_3$ nanoparticles were unsuccessful.

[27] M. Remškar, A. Mrzel, M. Viršek, A. Jesih, *Adv. Mater.* **2007**, *19*, 4276 – 4278.

[28] C. Perrin, M. Sergent, *J. Chem. Res. Synop.* **1983**, *2*, 38.

[29] U. Hotze, M. Binnewies, *Z. Anorg. Allg. Chem.* **2005**, *631*, 2467 – 2474.

[30] G. L. Frey, R. Tenne, M. J. Matthews, M. S. Dresselhaus, G. Dresselhaus, *Phys. Rev. B* **1999**, *60*, 2883 – 2892.

[31] J. A. Wilson, A. D. Yoffe, *Adv. Phys.* **1969**, *18*, 193 – 335.

[32] H. Schäfer, *Angew. Chem.* **1976**, *88*, 775 – 789; *Angew. Chem. Int. Ed. Engl.* **1976**, *15*, 713 – 727.

[33] L. Zhang, M. D'Acunzi, M. Kappl, G. K. Auernhammer, D. Vollmer, C. M. van Kats, A. van Blaaderen, *Langmuir* **2009**, *25*, 2711 – 2717.

[34] J. L. Feldman, *J. Phys. Chem. Solids* **1976**, *37*, 1141 – 1144.

[35] I. Kaplan-Ashiri, S. R. Cohen, G. Gartsman, R. Rosentsveig, G. Seifert, R. Tenne, *J. Mater. Res.* **2004**, *19*, 454 – 459.

[36] a) K. Lee, B. Lukic, A. Magrez, J. W. Seo, G. Andrew D. Briggs, A. J. Kulik, L. Forro, *Nano Lett.* **2007**, *7*, 1598 – 1602.

[37] Y. Q. Zhu, T. Sekine, Y. H. Li, W. X. Wang, M. W. Fay, H. Edwards, P. D. Brown, N. Fleischer, R. Tenne, *Adv. Mater.* **2005**, *17*, 1500 – 1503.

[38] R. Pfeiffer, M. Holzweber, H. Peterlik, H. Kuzmany, Z. Liu, K. Suenaga, H. Kataura, *Nano Lett.* **2007**, *7*, 2428 – 2434.

[39] a) N. Bertram, J. Cordes, Y. D. Kim, G. Ganteför, S. Gemming, G. Seifert, *Chem. Phys. Lett.* **2006**, *418*, 36 – 39; b) S. Gemming, J. Tamuliene, G. Seifert, N. Bertram, Y. D. Kim, G. Ganteför, *Appl. Phys. A* **2006**, *82*, 161 – 166.

